Annealing of bismuth telluride-based thick films by laser irradiation

Matteo d'Angelo [*], Dario Crimella, Carmen Galassi, Nora Lecis, Ali Gökhan Demir

Department of Mechanical Engineering, Politecnico di Milano, Milan 20156, Italy

A R T I C L E   I N F O

A B S T R A C T

Interest towards fabrication and post-processing of thermoelectric micro-sized devices has increased in recent years. The coupling of inexpensive deposition technologies and fast laser treatments on "as-deposited" films is an attractive solution for industrial scalability. In this work, we propose an approach never reported before in literature: the utilization of a ns-pulsed active fibre laser to directly densify p-type bismuth telluride-based thick films deposited on silicon. A feasibility study was conducted on the material to determine optimal laser parameters: the treated products were characterized, and it was concluded that a value of laser fluence as low as 4.5 mJ cm^{-2} is sufficient for densification. The material resulted cracked after the laser treatment, and it was demonstrated by SEM and profilometric analyses that shrinking occurs and sintering necks are formed; further, the arising of second phases after annealing was excluded by means of XRD analysis. Envisioning an industrial large area process with linear diode arrays source, a prediction of the laser power requirements to irradiate 1 mm^2 films in selected conditions is presented. More extensive studies will be performed to determine a narrower parameters window and determine a relationship between the film thickness and laser parameters for future applications to as-deposited films.

1. Introduction

The utilization of direct printing technologies for the preparation of small-scale electronic devices has increased in recent years thanks to their low cost, flexibility, and scalability. These technologies are often ink-based, where a slurry or a suspension is used to deposit a functional material with a certain pattern determined by a computer-aided design (CAD) model. The fabrication of micro-sized energy harvesters by direct printing has recently raised much interest in research, especially for thermoelectric devices thanks to their flexibility in the Internet of Things scenario [1–3]. Thermoelectric generators (TEGs) are electronic devices for solid-state energy harvesting: when a temperature gradient (ΔT) is applied to the opposite ends of a TEG, power is generated according to this temperature difference (the power generated therefore increases linearly with ΔT). TEGs allow the direct conversion of waste heat into electrical energy; a quiet and lightweight energy source without moving parts and free of green-house gas emissions. The efficiency of these devices is evaluated by the thermoelectric figure of merit ZT, that is calculated depending on the operational temperature (T, measured in K), the Seebeck coefficient (S, measured in μV K^{-1}), the electrical conductivity (σ, measured in S m^{-1}), and the thermal conductivity (k, measured in W m^{-1} K^{-1}) of the material: $ZT = S^2 \cdot \sigma \cdot T \cdot k^{-1}$ [4]. The main issue that research is facing right now is the low efficiency of the thermoelectric devices; it was determined that the minimum ZT value of a TE device to operate

---

* Corresponding author.
  E-mail address: matteo.dangelo@polimi.it (M. d'Angelo).

should be at least 1, where the highest commercial thermoelectric modules reach peaks of 1/1.1. The apparently opposite trend between electrical conductivity and thermal conductivity is the origin of such difficulties, given that an upper limit to ZT has not been defined yet: the increase of one of the two parameters leads to the increase of the other, thus counterbalancing the effects. The most efficient commercial modules are based on p-type and n-type bismuth telluride (Bi_2Te_3) legs; this material has the highest performance close to room temperature, as well as the highest raw material availability and lower production costs, compared to the other chalcogenides [4,5]. Further, in the last 30 years it has been experimentally demonstrated the abrupt increase in the thermoelectric performance when operating at micro- or nanoscale; therefore, the interest towards spot cooling or energy harvesting by using micro-thermoelectric devices is rapidly increasing [6]. The problem in deposition of micro-scale TEGs based on bismuth telluride with different technologies has been approached in literature several times (thickness from hundreds of nanometers to tens of micrometers), however there is a gap in regard to annealing of the films [7–10]. The state-of-the-art on post-treatment of bismuth telluride-based films is limited to thermal annealing: many studies have demonstrated its crucial role on electrical properties and microstructural homogeneity. However, the easiness in thermal annealing brings some drawbacks: the high vapor pressure of tellurium leads to its evaporation (i.e., the process is usually carried out in inert atmosphere from 400 to 500 °C) and low process scalability due to the difficult replicability of the results [11–14]. Tellurium loss has been partially solved by using pulsed-laser deposition technology with engineered targets that are enriched in Te to counterbalance this effect [15–18]. Anyhow, this technology is not scalable since it requires long and expensive thermal treatments after deposition to achieve similar properties to bulk materials, as well as expensive laser equipment and energy consumption, resulting in low process yield. Laser annealing consists in transferring energy to a material by laser irradiation and can be used either to melt and resolidify a material to obtain a dense product, or to modify the surface physical properties of metals or ceramic materials. Laser annealing is usually performed with laser fluence up to 10 mJ cm^{-2} and the outcome of the process depends on the target material physical properties (e.g., melting point, density) [19,20]. However, laser irradiation has favorable outcomes on many compounds, such as attainment of bulk-like properties after deposition and microstructural homogenization [21–23]. Fan et al. [24], rapidly grew a stoichiometric Bi_2Te_3 thin film by laser annealing a bulk target fabricated by thermal evaporation employing a CO_2 RF laser with frequency set at 30 kHz and laser fluence up to 6.6 mJ cm^{-2} using an irradiation time of 10 s. The layered target was composed by Te and Bi stacked layers with micrometric thickness (Te:Bi 2:1 thickness ratio to compensate for Te evaporation). They achieved 75 mm^2 area films and their crystalline properties depended on the laser parameters. The exceptional feature of this research work is the absence of thermal treatment after deposition. Anyhow, laser technology is here applied to a thermal evaporated target and not to an as-deposited film. This limits the process applicability to the fabrication of the films. There is a gap in literature regarding the utilization of laser annealing as a post processing technology associated with alternative fabrication technologies (e.g., direct ink printing), and not as the final step of a fabrication technology merged with annealing. The possibility to directly anneal thick films by simple laser equipment right after deposition is an attractive solution to speed up and scale production of small-size thermoelectric devices. This approach was already attempted on other materials, giving credit to this possibility. Nazarenus et al. [25], successfully achieved bulk-like thermoelectric properties on $CuFe_{0.98}Sn_{0.02}O_2$ thick films (thickness of several micrometers) deposited by powder aerosol deposition (PAD); the films were laser annealed rather than using a conventional heat-treatment. PAD has many common advantages among most deposition technologies: low cost, easy and fast fabrication of thick films on any substrate using any material; after deposition, an annealing post-treatment is always necessary to attain bulk-like properties. They used a Nd: YAG laser with a wavelength of 355 nm with penetration depth around 1 μm. The film showed high homogeneity and crystallinity after
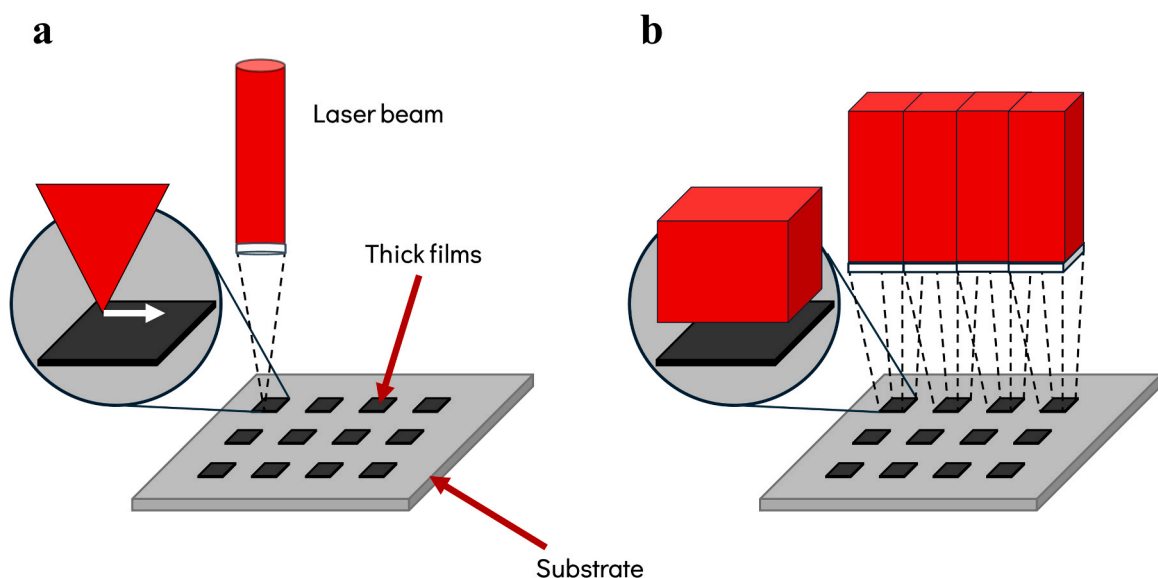

Fig. 1. a) Representation of the annealing process using the ns-pulsed fibre laser with direct writing using a scanner head b) Representation of the possible industrial scale up of the process using a square-shaped beam and linear diode array laser source.

the treatment, as well as an increase of electrical conductivity by three orders of magnitude. Therefore, literature validates this approach as an efficient way to anneal functional thick films. In this work, a p-type bismuth telluride-based thick film deposited by spin coating on a silicon/silicon dioxide substrate was annealed by laser irradiation using a scanner head in a direct writing configuration (Fig. 1a). To the best knowledge of authors, chalcogenides-based films were never laser annealed before and this work can be considered as a first-time-try of this process. A ns-pulsed active fibre laser was used in inert argon atmosphere, and 36 different parameters combinations were tested following literature approaches as starting ground [26]. The conditions were designed to transfer relatively small energy to the film due to the low melting point of bismuth telluride alloys (610 °C for the $Bi_{0.5}Sb_{1.5}Te_3$ alloy [27]); this was done by fixing a large distance from the focal point of the laser as well as using low laser average power. Optical and scanning electron microscope analyses revealed that shrinking and densification of the material take place following laser irradiation; the film does not appear as completely densified, indicating that an optimization of the parameters window is crucial. Further, optical profilometry was performed to determine the depth of the cracks and estimate the laser penetration length through the film. X-Ray diffraction analysis showed that following annealing, the material did not undergo the formation of second phases; further, laser treatment is so fast that the orientation of material is not possible, and therefore cannot be detected by XRD analysis. In conclusion, the annealing tests should be continued on 1 mm × 1 mm area films to understand whether inhomogeneities derive from the expansion mismatch of the film or due to rapid cooling during treatment [25]. Large area application of this process must be studied to promote a possible industrial scale-up; the utilization of a laser with linear diode arrays source for material annealing is a solution when used to selectively anneal multiple films contemporarily (Fig. 1b). At this aim, a prediction of energy density and irradiance in optimal conditions using a square shaped and wider beam is presented. The final objective is to determine a relation between the laser parameters and the film thickness to attempt the industrial scale-up and coupling with direct ink writing. It is worth remarking that in this work we demonstrate the feasibility of the process showing the annealed film, highlighting also the many open points in this first-time application of laser technology, that will be tackled in future works.
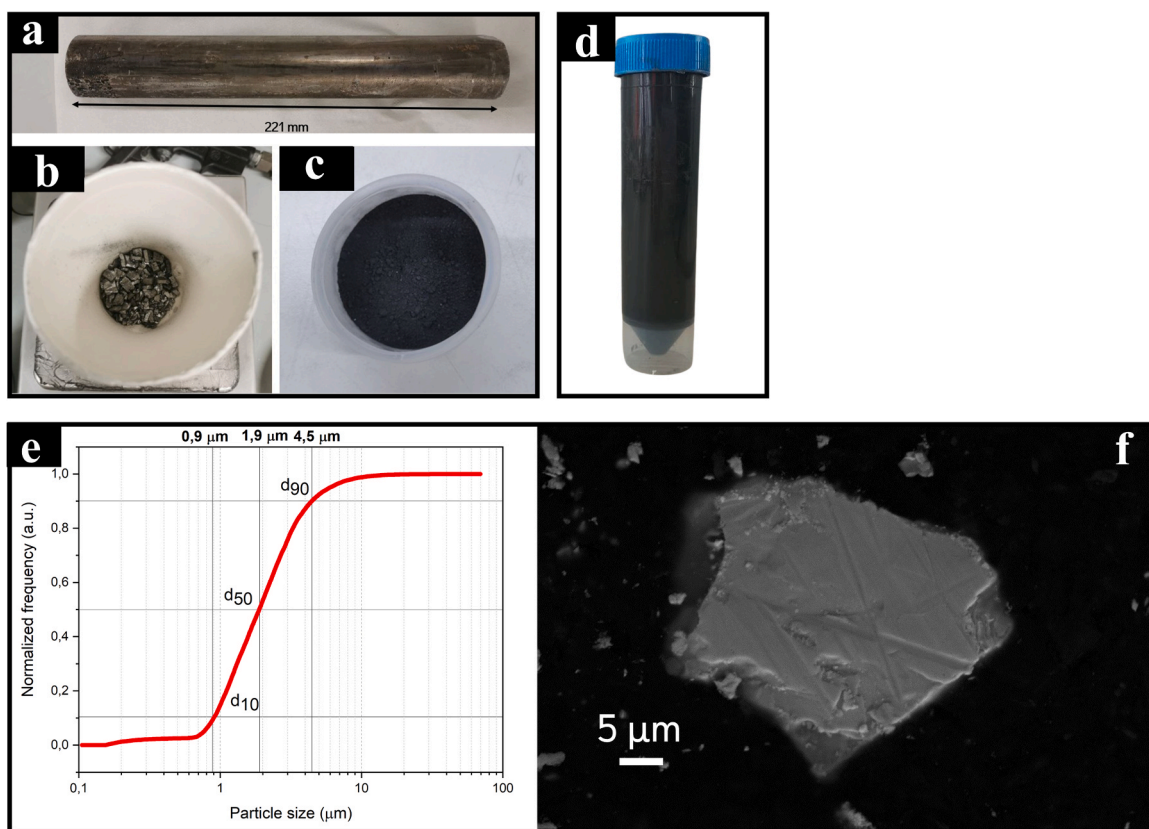

Fig. 2. a) The pristine p-type ingot. b) The ingot right after hand grinding. c) The powder after the standard ball milling process. d) The ink with 10 %wt p-type powder in ethanol with 1 %wt Lubrizol Solsperse AC4320. e) The normalized frequency vs particle size (μm) curve of the powder used to prepare the ink: the analysis was performed using Malvern Morphologi 4. f) SEM image of a large particle of the ball milled batch where the irregular morphology of the powder is evident.

2. Materials and methods

2.1. Preparation of the suspension for spin coating

The p-type bismuth telluride powder for the preparation of the suspension for spin coating was prepared by grinding the $Bi_{0.4}Sb_{1.6}Te_3$ ingot supplied by MeTek. The ingot was initially hand crushed, and then ball milled (Retsch planetary mill PM400) in a 250 cc zirconia jar filled with argon using zirconia spheres (Ø 5 mm, 6 hours at 400 rpm with 2 min milling and 1 min holding time); the powder was handled in argon-filled glovebox (the original ingot, the hand grinded material and the milled powder are depicted from Fig. 2a–c, respectively. The energy dispersive spectroscopy analysis of the pristine ingot is reported in Table 1). The central diameter of large part (d_{90}) of the powder was around 4.5 μm (the granulometric analysis is depicted in Fig. 2e) and its morphology is irregular (a scanning electron microscope image is depicted in Fig. 2f). A suspension was prepared by dispersing 10 %wt solid fraction of powder in the solution of Lubrizol Solsperse AC4320 (1 %wt to powder mass) in ethanol (Carlo Erba anhydrous ethanol absolute, 1 mL g^{-1} powder). The suspension was homogenized in a trundler at 150 rpm with zirconia spheres (Ø 5 mm) for 16 hours; the ink is depicted in Fig. 2d.

2.2. Preparation of the substrate and spin coating

The deposition was carried out on silicon/silicon dioxide substrates (thickness 725 μm) that were cleaned and activated before spin coating. Substrates cleaning was done by sonicating for 10 min in acetone, and then rinsing in absolute ethanol; the activation was done in oxygen plasma using Diener Electronic ATTA (3 min of treatment). Spin coating was performed using the spin coater MODEL WS-650SZ-8NPP/lite and was done by a double step deposition: in the first one the suspension was spinned for 60 s at 400 rpm, and in the second step spinning was carried out for 30 s at 200 rpm. The films were dried in air at room temperature, and then treated with laser irradiation.

2.3. Laser system

Laser irradiation was performed using a ns-pulsed active fiber laser (IPG Photonics, YLP-1/100/50/50, Cambridge, MA, USA). The system was coupled to a scanner head equipped with a 100 mm f-theta lens for beam steering and focusing (Sunny Technology TSH 8310, Beijing, China). The laser system is depicted in Fig. 3 and the characteristics of the laser source are summarized in Table 2.

Throughout the experiments 20 kHz pulse repetition rate was used because of the low melting point of bismuth telluride. The laser average power (P_{avg}), the focal point (Δz) of the beam, the scan speed (v) and the hatch distance (h) between consecutive scan lines were varied. All experiments were carried out using an argon flux through a custom-made Plexiglass set-up to simulate inert atmosphere. The beam size at the tested conditions (d_s) corresponding to $\Delta z = 3$ mm and $\Delta z = 4$ mm were 181 and 239 μm, respectively. The laser was used to anneal 1×1 mm square spots on the 20 mm × 20 mm spin-coated film. The serpentine laser strategy was adopted to cover the whole 1 mm^2 area. The fixed and varying experimental parameters are summarized in Table 3.

For this study, we also compared the laser fluence (F, mJ cm^{-2} in Eq. (1)) used for annealing the film in the different conditions [28].

$$F = \frac{8E}{\pi d_s^2} \tag{1}$$

Where E is the ratio between the average laser power and the pulse repetition rate ($E = \frac{P_{avg}}{PRR}$).

2.4. Characterization

The sintered film was analyzed by optical microscopy (OM, Nikon Eclipse LV150LN), field emission scanning electron microscopy (FE-SEM, Zeiss sigma 500), energy dispersive spectroscopy (EDS, Zeiss sigma 500), optical profilometry (OP, Mahr MarSurf CWM 100 and Alicona Suite 5.3.2), and X-ray diffraction (XRD) analysis (Rigaku SmartLab).

Reproducibility of the results was ensured by treating one spin coated sample (20 mm × 20 mm, Fig. 4) with homogeneous thickness and repeating the same conditions multiple times. The spin coated sample was previously characterized by optical profilometry to determine the average thickness (∼ 27 μm) and homogeneity.

Table 1
EDS analysis in atomic fraction of the $Bi_{0.4}Sb_{1.6}Te_3$ pristine ingot.

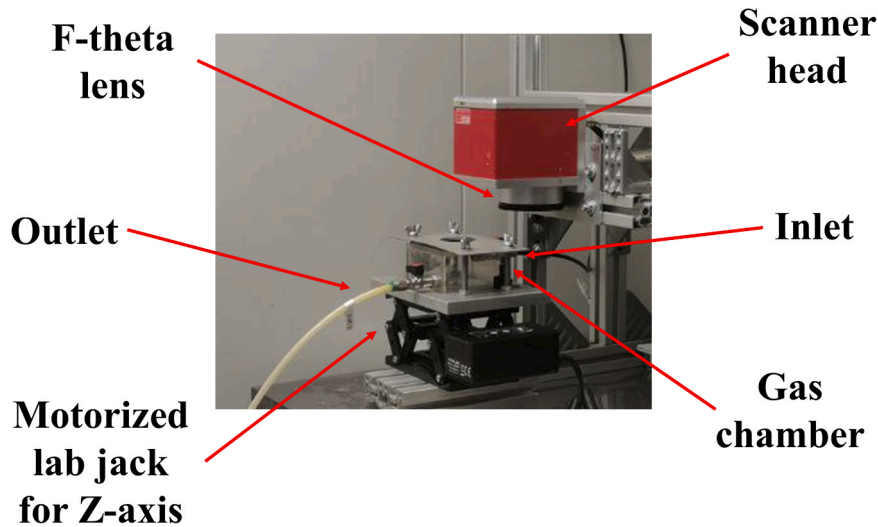| Element	Content %at.
Bi	11
Sb	29
Te	60

Fig. 3. The laser system is depicted with its main components.

Table 2
The general characteristics of the pulsed laser source are summarized.

Parameters	Symbol	Value
Wavelength	λ	1064 nm
Max. average power	P_{avg}	50 W
Pulse duration	τ	250 ns
Pulse repetition rate	PRR	20–80 kHz
Max. pulse energy	E	1 mJ
Beam	M^2	1.7
Collimated beam diameter	d_C	5.9 mm
Focal length	f	100 mm
Focused beam diameter	d_0	39 μm

Table 3
Fixed and varying parameters for the experimental campaign.

Fixed parameters	Level
Pulse Repetition Rate, PRR (kHz)	20
Number of laser passes, N	1
Shielding gas	Ar at 0.5 bar
Varied parameters	**Levels**
Transversal speed, v (mm s^{-1})	5, 25, 50
Average power, P_{avg} (mW)	10, 20, 40
Focal position, Δz (mm)	3, 4
Hatch distance, h (μm)	10, 50

3. Results and discussion

3.1. Definition of the quality levels and process feasibility

Following the laser treatment, three different outcomes were identified: slight modification (Fig. 5a), superficial aspect of the film not changed drastically (Fig. 5b), or total removal of the material (Fig. 5c). The first and last cases are a consequence of incorrect laser parameters, instead the case in Fig. 5b results from acceptable conditions.

The feasibility study was performed to determine the best processing conditions, and it was limited to three different energy levels (P_{avg} = 10, 20 and 40 mW), three different velocities (v = 5, 25 and 50 mm s^{-1}), and two different hatch distances (h = 10 and 50 μm), as reported in Table 3.

Two different studies were carried out at fixed focal distance (Δz = 3 and 4 mm), fixed pulse repetition rate (PRR = 20 kHz), and with single laser pass for a total of 36 different conditions; the graphical representation of the feasibility study with focal distance of 3 mm and 4 mm are captured in Fig. 6a and b, respectively. The three conditions identified in Fig. 4 were transposed in two conditions
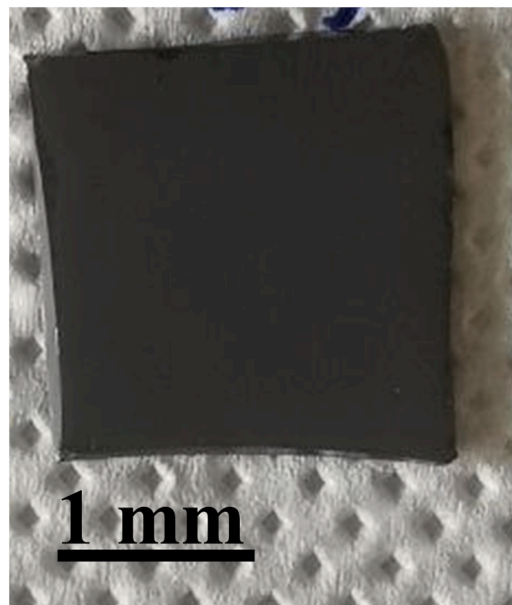
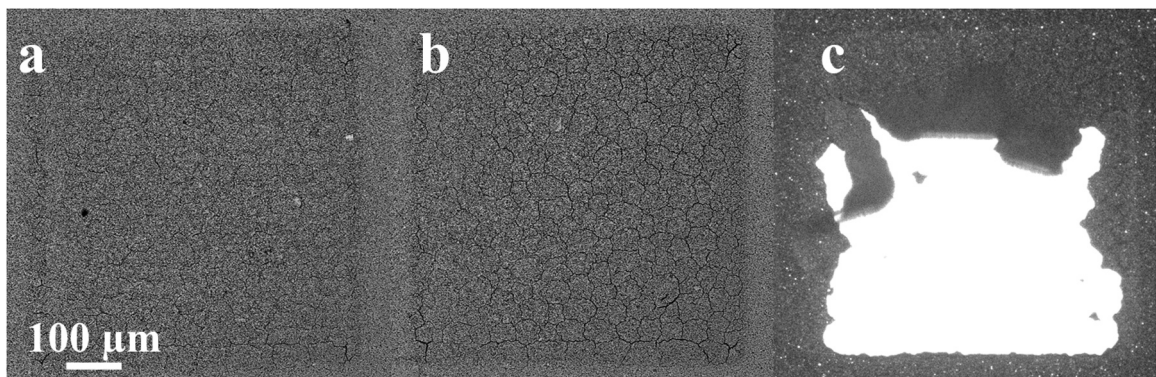**Fig. 4.** The spin coated sample right after printing.

Fig. 5. SEM images of the films after laser irradiation showing conditions of: a) non-annealed (P_{avg} = 10 mW, v = 5 mm s^{-1}, Δz = 3 mm, h = 10 μm, PRR = 20 kHz and single laser pass), b) annealed (P_{avg} = 20 mW, v = 5 mm s^{-1}, Δz = 3 mm, h = 10 μm, PRR = 20 kHz and single laser pass), and c) damaged (P_{avg} = 40 mW, v = 5 mm s^{-1}, Δz = 3 mm, h = 10 μm, PRR = 20 kHz and single laser pass) conditions.
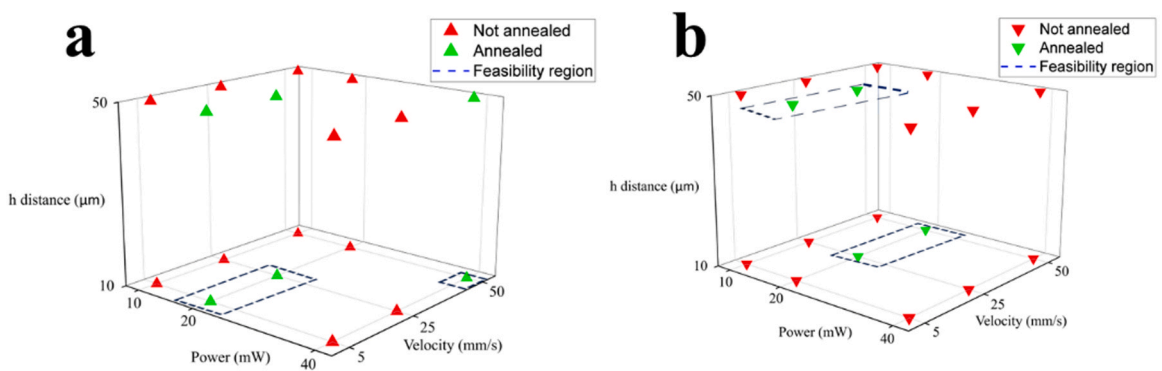

Fig. 6. a) Feasibility study at focal distance of 3 mm. b) Feasibility study at focal distance of 4 mm. Both studies must be considered at single laser pass and at fixed pulse repetition rate (PRR) of 20 kHz.

in the feasibility study: the red triangles represent non-densified samples (like in Figs. 5a and 5c), and the green triangles are associated with densified samples (like in Fig. 5b).

An optical microscope image for each single condition is shown in Fig. 7 [28], where the figures highlighted in green correspond to
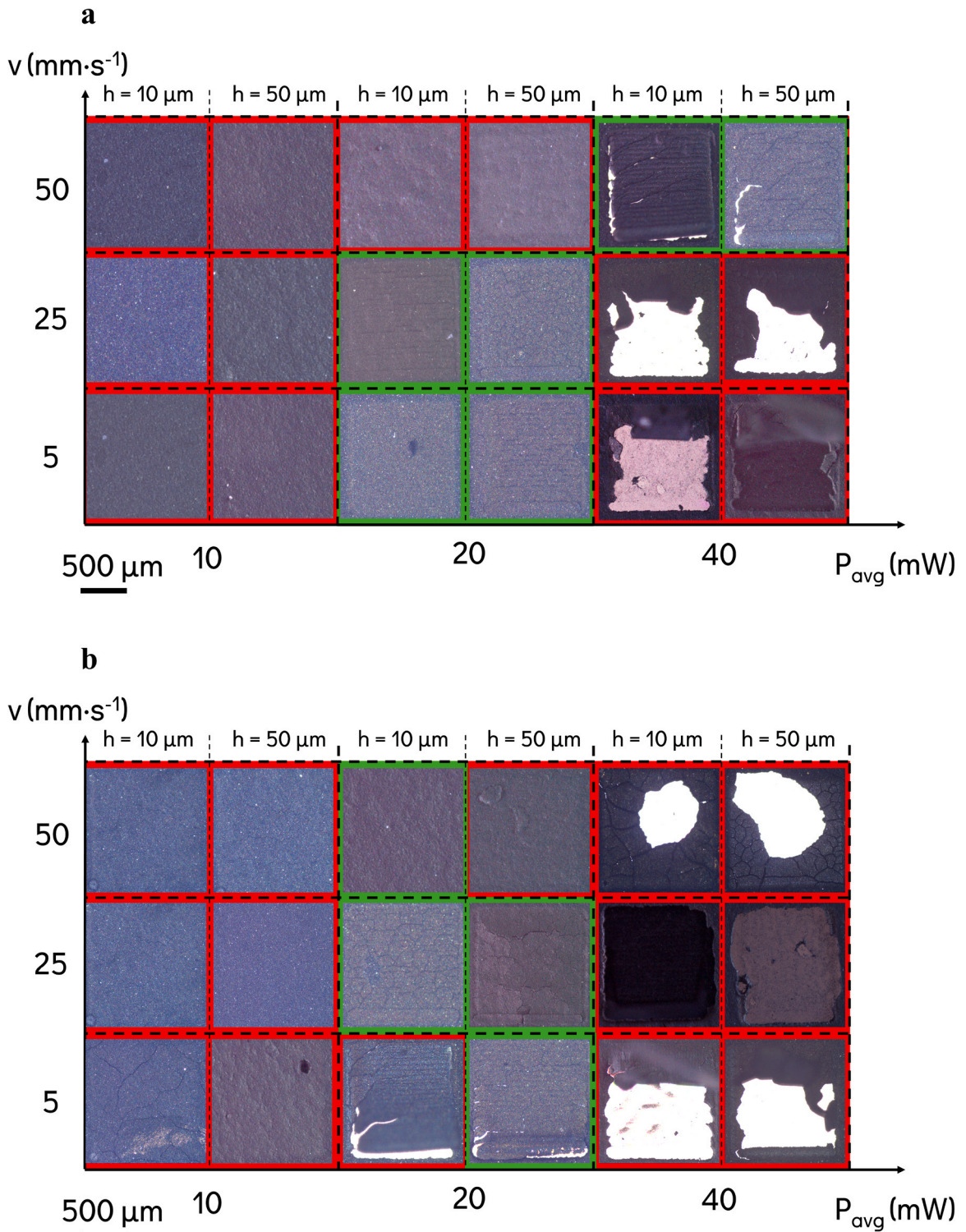

Fig. 7. OM images of the surface of the films resulting from the 18 different conditions at $\Delta z = 3$ mm (a), and at $\Delta z = 4$ mm (b). These images are to be considered at PRR = 20 kHz and single laser pass.

the densified samples. The films annealed in best conditions show a network of fine cracks on the surface, that were attributed to the stress mismatch due to shrinking after densification.

In this work, we laser irradiated the bismuth telluride-based thick film to attain the densification of the material: since it was never attempted before it was necessary to screen different conditions and we expected to define a set of parameters where densification takes place. The seven suitable laser parameters combinations for annealing are summarized in Table 4. The unsuccessful laser irradiation of the films at power of 10 mW (i.e., laser fluence of 3.9 and 2.3 mJ cm^{-2}, respectively for the tests at focal distance of 3 and 4 mm) was attributed to the low energy of the laser beam; the low laser velocity (5 mm s^{-1}) was selected to increase the laser residence time on the material and achieve densification but without success. The utilization instead of the highest laser power of 40 mW led to large energy transfer to the film resulting in irreversible material degradation. In some cases, the 40 mW power led to acceptable results in combination with the high speed of 50 mm s^{-1}, independently from the hatch distance; it might have allowed to mitigate the effect of the laser. Further, the hatch distance is a parameter that does not play a crucial role over the final microstructure since acceptable result were achieved either in the smallest and largest hatch distance. In all conditions, larger cracking of the film occurs when irradiated at higher focal distance; in the selected conditions the best result is achieved with $\Delta z = 3$ mm. Finally, the optimal laser velocity is found in the proximity of 25 mm s^{-1}, the acceptable results achieved at 5 or 50 mm s^{-1} where not reproducible and are not considerable reliable.

Therefore, minimum laser fluence for achieving densification is 4.5 mJ cm^{-2}, which is less than half of the most common laser treatment processes.

3.2. Analysis of the annealed films

The morphology of the areas of the film irradiated by the laser was studied by optical profilometry, whereas the pristine spin coated film is compared to the irradiated one (Fig. 8). Only the samples summarized in Table 4 were analyzed, given the low quality in the other cases.

The samples annealed the seven selected conditions show some superficial cracks due to the stress mismatch between the annealed part and the "as-deposited" part. The cracks do not penetrate the full thickness of the film, just reaching a top depth of 2 μm; these inhomogeneities are considered as the visible and direct consequence of annealing on the samples. It is also possible that crack formation happens as a result of combining the shrinking and the rapid cooling due to the laser treatment, as highlighted by Nazarenus et al. [25]. The cracks penetration extent is comparable to the laser penetration depth, but the annealing extent cannot be evaluated in such way since the heat transferred by the beam is cause of densification; this aspect of the annealed films should be deepened by transversal SEM analysis.

Another proof of efficient annealing is the absence of material removal on the film, indicating that the laser treatment is not working like a subtractive technology (e.g., laser ablation) but as a densification process (the film thickness before and after treatment is unchanged). The most visible difference is the presence of sharp negative peaks in the profile due to cracking, that are not present prior to irradiation. The high steepness of the cracks is due to the surface tension on the film after shrinking.

This last point was also proved by SEM analyses: the high magnification images on the as-deposited film compared to the sintered film are different (Fig. 9). In the latter case the particles are closer than in the former, showing sintering necks that evidence at least a partial densification. The low densification extent is evidenced also by large residual porosity in the film. Furthermore, it appears that the densification of the film takes place preferentially following the direction of the laser pass, probably due to the heat distribution over the film during irradiation. It is also noticeable the difference between the particles far from (Fig. 8a) and close to (Fig. 8b) the annealed area: the particles on the "as-deposited" film do not show any sign of densification, whereas the edges show some densified particles. This is also an indication that heat transfer from the treated area occurs and favors densification, however without a large spreading of the process due to the low thermal conductivity bismuth telluride as compared to other materials (e.g., metals).

EDS analysis revealed that the films did not underwent oxidation (Table 5), the argon chamber prevented the formation of oxides; the amount of carbon and oxygen is due to the residual binder. Further, tellurium content before and after irradiation is unchanged meaning that tellurium evaporation is not taking place due to the lower energy transferred to the material compared to conventional annealing procedures.

The films were analyzed by means of XRD analysis both before and after annealing with the latter subjected to selected conditions ($P_{avg} = 20$ mW, $v = 25$ mm s^{-1}, $h = 10$ μm, and $\Delta z = 3$ mm, with laser fluence of 7.8 mJ cm^{-2}). The XRD analysis was performed in the range from 10° to 60° with a scan speed of 1° min^{-1}, using a tube potential and current of 20 kV and 2 mA, respectively. The low potential and current were used because of the small thickness of the films, and therefore to avoid the detection of the underlying Si/

Table 4
The seven selected conditions at fixed PRR of 20 kHz and single laser pass.

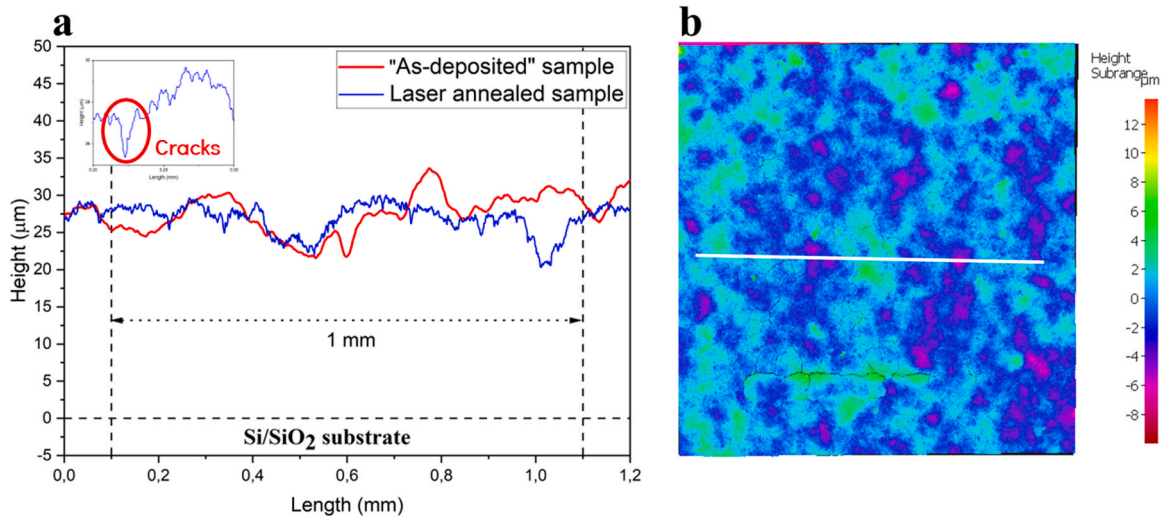| Parameters at $\Delta z = 3$ mm				Parameters at $\Delta z = 4$ mm			
P_{avg} (mW)	v (mm s^{-1})	h (μm)	F (mJ cm^{-2})	P_{avg} (mW)	v (mm s^{-1})	h (μm)	F (mJ cm^{-2})
20	5	50	7.8	20	5	50	4.5
20	25	50	7.8	20	25	50	4.5
20	5	10	7.8	20	25	10	4.5
20	25	10	7.8	20			

Fig. 8. a) Optical profilometry of the pristine spin coated sample compared with the profilometry of a sample annealed with $P_{avg} = 20$ mW, $v = 25$ mm s^{-1}, h = 10 μm, and Δz = 3 mm (laser fluence of 7.8 mJ cm^{-2}). Further, a zoom in of the cracked areas is shown. b) Profilometric heat map of the film, with the white line representing the profiling direction.
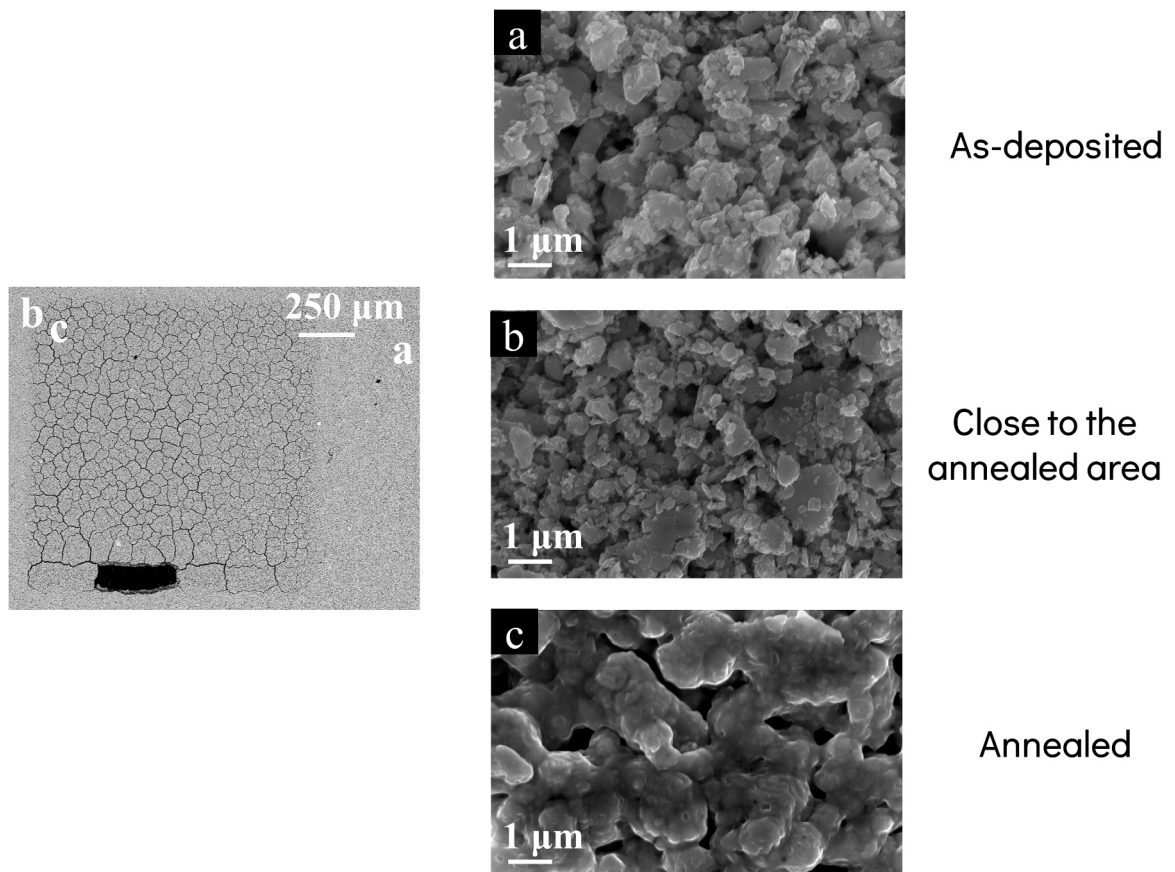

Fig. 9. The sample annealed with $P_{avg} = 20$ mW, $v = 25$ mm s^{-1}, h = 10 μm, and Δz = 3 mm (laser fluence of 7.8 mJ cm^{-2}) was analyzed by means of FE-SEM analysis. a) SEM image of the "as-deposited" film. b) SEM image on the edge of the annealed area. c) SEM image of the sample within the annealed area.

Table 5
Results of the EDS analysis performed on the sample annealed with $P_{avg} = 20$ mW, $v = 25$ mm s^{-1}, $h = 10$ μm, and $\Delta z = 3$ mm, where area a, b and c refer to Fig. 8.

Element	Composition		
	Area a wt%	Area b wt%	Area c wt%
Bi	16.4	16.6	16.5
Sb	23.3	23.1	23.3
Te	51.9	52.3	53.9
C	4.4	4.2	3.9
O	4.0	3.8	2.4

SiO_2 substrate. Initially, the analysis was carried out up to 80 ° but the reflections of bismuth telluride were not distinguishable due to the high intensity of the of SiO_2 reflection at 69° (id #9009238 COD); further, the characteristic reflections of $Bi_{0.4}Sb_{1.6}Te_3$ are comprised in the range from 10° to 60°. The comparison between the two spectra is depicted in Fig. 10. The reflections of the most formed oxides of bismuth (i.e., Bi_2O_3), tellurium (i.e., TeO_2) and antimony (i.e., Sb_2O_3) are not visible in the spectra. Further, pure tellurium phases are not detected, which indicates that the treatment did not lead to melting and phase separation, which happens often in conventional post-processing treatments. In the 10–60° diffraction angle range, just two weak reflections of the SiO_2 phase (if #90092338 COD) of the underlying substrate were detected at 33° and 46°, respectively. All the other reflections are relative to the rhombohedral $Bi_{0.4}Sb_{1.6}Te_3$ phase (id #1530822 COD), which is consistent with the designed composition of the film, nonetheless the reflections intensity is identical in the two cases. Therefore, it is concluded that after densification the material did not undergo any changes in its composition, and secondary unwanted phases are not formed (e.g., oxides or pure tellurium phases). The material does not show any sign of orientation after annealing both due to the high speed of the treatment, and the inherent random distribution of the particle typical of spin coated films.

3.3. Preliminary analysis of process scale-up

Although the preliminary results show that the process requires more attention to improve quality, a forecast for large area annealing applications can be made. For this purpose, the energy density (E) over the scanned area and the average beam irradiance (I) area can be calculated as [26]:

$$E = \frac{P_{avg}}{vh} \tag{2}$$

$$I = \frac{P}{\frac{d_s^2}{4}\pi} \tag{3}$$

The irradiation parameters of the selected condition for this analysis are $P_{avg} = 20$ mW, $h = 10$ μm, $v = 25$ mm s^{-1}, $\Delta z = 3$ mm and PRR = 20 kHz with one single laser pass: the energy density and average irradiance are 80 J cm^{-2} and 44.5 W cm^{-2}, respectively. The process can be envisaged to employ a square shaped and wider beam with diode laser sources having a similar emission wavelength (e. g., 980 nm). Assuming a 1 mm edge size (a) of a square shaped beam, the process could be potentially carried out by employing 1.6 W power at 0.5 s exposure time (t) without moving the beam, while producing the same energy density ($E = Pt \cdot a^{-2}$) and irradiance ($I = P \cdot a^{-2}$) outputs. This implies that linear diode arrays with each beam having the calculated properties can be potentially employed for wide area processing in a selective manner [29].

4. Conclusions

Laser annealing of p-type bismuth telluride-based thick films is possible, and we achieved densification of the material by laser irradiation for the first time; however, parameters optimization is a crucial step to implement this annealing technology on direct ink writing systems. The minimum laser fluence to densify the $Bi_{0.4}Sb_{1.6}Te_3$ film is 4.5 mJ cm^{-2}, and the suitable conditions are power 20 mW, hatch distance between 10 and 50 μm, laser velocity close to 25 mm s^{-1}, and a focal distance comprised between 3 and 4 mm (using single laser pass and with pulse repetition rate of 20 kHz). Film degradation takes place when the employed laser power is 40 mW, as well as using laser power of 10 mW leads to no changes of the material. Further, too large laser velocity reduces drastically the laser residency time leading to unmodified film after irradiation. The effectiveness of the process was proved by SEM analysis; the cracked areas showed that the particles are closer, and in many cases, with visible sintering necks. The cracks depth does not exceed 2 μm, and material removal does not occur, revealing that the process does not act as a subtractive technology. Further, XRD analysis revealed that the material did not present any secondary phases after laser annealing (e.g., due to the formation of oxides and/or pure tellurium), as well as not showing any specific preferential orientation after treatment, which is due to the high velocity of the process and the inherent lack of orientation of the deposition technology. Compared to conventional technologies, the formation of pure tellurium or oxides was avoided still achieving partial material densification.

An industrial process in which a linear diode array laser source is used to selectively anneal different films contemporarily can be
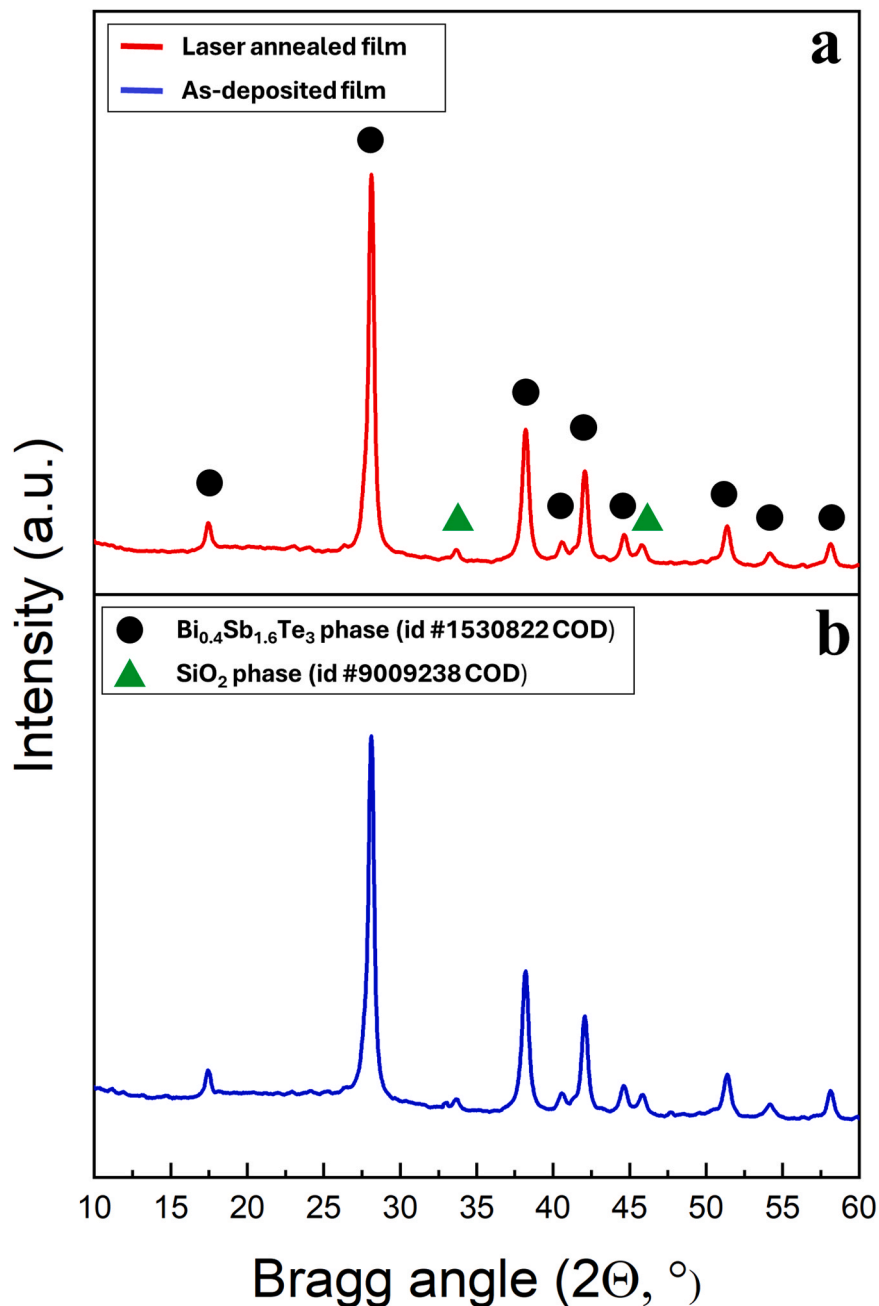
Fig. 10. a) XRD spectrum of the film laser annealed at $P_{avg} = 20$ mW, $v = 25$ mm s^{-1}, $h = 10$ μm, and $\Delta z = 3$ mm (laser fluence of 7.8 mJ cm^{-2}). b) XRD spectrum of the as-deposited film.

envisaged; at this aim a prediction of the process in suitable conditions for the irradiation of 1 mm^2 films is also presented. Film annealing can be achieved with 1.6 W power and 0.5 s exposure time, considering the utilization of a square shaped and larger beam with diode laser source. The order of units of Watts is very low and promising for a possible industrial scale-up.

Further experimental activity should aim at studying the crack formation mechanism on the film, compare the charge mobility and electrical resistivity of the material before and after annealing, and finally to define a narrower parameters window to improve the treated material quality and to promote possible application of this technology to films deposited with other technologies.

The final aim of this study is to determine a relation between the laser parameters and the film thickness to implement this technology in an industrial scenario.

CRediT authorship contribution statement

Dario Crimella: Supervision, Methodology, Investigation. **Matteo d'Angelo:** Writing – review & editing, Writing – original draft, Methodology, Investigation, Data curation, Conceptualization. **Nora Lecis:** Writing – review & editing, Supervision, Funding acquisition. **Carmen Galassi:** Writing – review & editing, Supervision. **Ali Gökhan Demir:** Writing – review & editing, Writing – original draft, Supervision, Methodology.

Declaration of Competing Interest

The authors declare that they have no known competing financial interests or personal relationships that could have appeared to influence the work reported in this paper.

Data availability

Data will be made available on request.

Acknowledgements

References

[1] M. Singh, H.M. Haverinen, P. Dhagat, G.E. Jabbour, Inkjet printing-process and its applications, Adv. Mater. 22 (2010) 673–685.
[2] F. Shao, Q. Wan, Recent progress on jet printing of oxide-based thin film transistors, J. Phys. D Appl. Phys. 52 (2019) 1–5.
[3] L.J. Deiner, T.L. Reitz, Inkjet and aerosol jet printing of electrochemical devices for energy conversion and storage, Adv. Eng. Mater. 19 (2017) 4–8.
[4] H.J. Goldsmid, Thermoelectrics and its Energy Harvesting, CRC Press, 2012 (vol. Edition 1).
[5] G. Liu, T. Wang, Research progress in thermoelectric materials for sensor application, Acta Chim. Sin. 75 (2017) 1029–1035.
[6] L.D. Hicks, M.S. Dresselhaus, Thermoelectric figure of merit of a one-dimensional conductor, Phys. Rev. B 47 (1993) 16631–16634.
[7] C. Hollar, Z. Lin, M. Kongara, T. Varghese, C. Karthik, J. Schimpf, J. Eixenberg, P.H. Davis, Y. Wu, X. Duan, Y. Zhang, D. Estrada, High-performance flexible bismuth telluride thin film from solution processed colloidal nanoplates, Adv. Mater. Technol. 5 (2020) 1–8.
[8] B. Hu, X. Shi, T. Cao, M. Li, W. Chen, W. Liu, W. Lyu, T. Tesfamichael, Z. Chen, Advances in flexible thermoelectric materials and devices fabricated by magnetron sputtering, Small Sci. (2023) 1–8 (n/d).
[9] O. Yamashita, S. Tomiyoshi, Effect of annealing on thermoelectric properties of bismuth telluride compounds, Jpn. J. Appl. Phys. 42 (2003) 492–499.
[10] H. Huang, W. Luan, S. Tu, Influence of annealing on thermoelectric properties of bismuth telluride films grown via radio frequency magnetron sputtering, Thin Solid Films 517 (2009) 3731–3734.
[11] M.L. Lwin, P. Dharmaiah, S. Yoon, S.H. Song, H.S. Kim, J. Lee, R. Ghomashchi, S. Hong, Correlation with the composition of the different parts of p-type $Bi_{0.5}Sb_{1.5}Te_3$ sintered bulks and their thermoelectric characteristics, J. Alloy. Compd. 845 (2020) 1–10.
[12] S.A. Haidar, Y. Gao, Y. He, J.E. Cornett, B. Chen, N.J. Coburn, C. Glynn, M.T. Dunham, K.E. Goodson, N. Sun, Deposition and fabrication of sputtered bismuth telluride and antimony telluride for microscale thermoelectric energy harvesters, Thin Solid Films 717 (2021) 1–9.
[13] D.H. Kim, I.H. Kwon, C. Kim, B. Han, H. Im, H. Kim, Tellurium-evaporation-annealing for p-type bismuth–antimony–telluride thermoelectric materials. J. Alloy. Compd. 548 (2013) 126–132.
[14] S. Li, H.M.A. Soliman, J. Zhou, M. Toprak, M. Muhammed, D. Platzek, P. Ziolkowski, E. Mueller, Effects of annealing and doping on nanostructured bismuth telluride thick films, Chem. Mater. 20 (2008) 4403–4410.
[15] A.E. Shupenev, I.S. Korshunov, A.G. Grigoryants, On the pulsed-laser deposition of bismuth-telluride thin films on polyimide substrates, Semiconductors 54 (2020) 378–382.
[16] A.A. Aziz, M. Elsayed, H.A. Bakr, J. El-rifai, T. Van der Donck, J. Celis, V. Leonov, P. Fiorini, S. Sedky, Pulsed laser deposition of bismuth telluride thin films for microelectromechanical systems thermoelectric energy harvesters, J. Electron. Mater. 39 (2010) 1920–1925.
[17] S. Higomo, T. Yagi, H. Obara, A. Yamamoto, K. Ueno, T. Iida, N. Taketoshi, T. Baba, Thermoelectric properties of Bi_2Te_3 based thin films fabricated by pulsed laser deposition. THERMOELECTRIC POWER GENERATION WE-Conference Proceedings Citation Index, vol. 1044, 2008, 389–+.
[18] P.H. Le, C.-N. Liao, C.W. Luo, J. Leu, Thermoelectric properties of nanostructured bismuth–telluride thin films grown using pulsed laser deposition. J. Alloy. Compd. 615 (2014) 546–552.
[19] P. Chen, M. Tsukamoto, in: Y. Setsuhara, T. Kamiya, S. Yamaura (Eds.), Surface Modification with Femtosecond Laser BT – Novel Structured Metallic and Inorganic Materials, Springer Singapore, 2019, pp. 469–483, https://doi.org/10.1007/978-981-13-7611-5_32.
[20] K.L. Pey, P.S. Lee, Pulsed laser annealing technology for nanoscale fabrication of silicon-based devices in semiconductors, in: J. Lawerence, J. Pou, D.K.Y. Low, E. Toyserkani (Eds.), Advances in Laser Materials Processing: Technology, Research and Applications, 2010, pp. 327–364, https://doi.org/10.1533/9781845699819.4.327.
[21] P.A. Podrabinnik, I.V. Shishkovsky, Laser post annealing of cold-sprayed Al–Ni composite coatings for green energy tasks. Procedia IUTAM 23 (2017) 108–113.
[22] M. Tsukamoto, N. Abe, Y. Soga, M. Yoshida, H. Nakano, M. Fujita, J. Akedo, Control of electrical resistance of TiO_2 films by short-pulse laser irradiation, Appl. Phys. A 93 (2008) 193–196.
[23] T. Shinonaga, S. Kinoshita, Y. Okamoto, M. Tsukamoto, A. Okada, Formation of periodic nanostructures with femtosecond laser for creation of new functional biomaterials, Procedia CIRP 42 (2016) 57–61.
[24] L. Fan, J. Tang, L. Wu, S. Zhang, F. Liu, J. Yao, L. Guo, Rapid growth of high-performance Bi_2Te_3 thin films by laser annealing at room temperature, Appl. Surf. Sci. 639 (2023) 1–7.
[25] T. Nazarenus, J. Kita, R. Moos, J. Exner, Laser-annealing of thermoelectric $CuFe_{0.98}Sn_{0.02}O_2$ films produced by powder aerosol deposition method, Adv. Mater. Interfaces 7 (2020) 1–13.
[26] L. Kotsedi, V. Furlan, V. Bharadwaj, K. Kaviyarasu, B. Sotillo, C.B. Mtshali, N. Matinise, A.G. Demir, B. Previtali, R. Ramponi, S. Eaton, M. Maaza, M, Chromium oxide formation on nanosecond and femtosecond laser irradiated thin chromium films, Opt. Mater. 95 (2019) 1–4.

[27] Y. Luo, J. Yang, Q. Jiang, L. Fu, Y. Xiao, W. Li, D. Zhang, Z. Zhou, Y. Cheng, Melting and solidification of bismuth antimony telluride under a high magnetic field: a new route to high thermoelectric performance, Nano Energy 15 (2015) 709–718.

[28] M. Colopi, L. Caprio, A.G. Demir, B. Previtali, Selective laser melting of pure Cu with a 1 kW single mode fiber laser, in: Proceedings of the 10TH CIRP Conference on Photonic Technologies [LANE 2018], vol. 74, 2018, pp. 59–63.

[29] M. Zavala-Arredondo, N. Boone, J. Willmott, D.T.D. Childs, P. Ivanov, K.M. Groom, K. Mumtaz, Laser diode area melting for high speed additive manufacturing of metallic components, Mater. Des. 117 (2017) 305–315.